Unveiling the underlying molecular basis of astaxanthin accumulation in *Haematococcus* through integrative metabolomic-transcriptomic analysis

Cristina Hoys [a,1], Ana B. Romero-Losada [a,b,1], Esperanza del Río [a], Miguel G. Guerrero [a,c], Francisco J. Romero-Campero [a,b], Mercedes García-González [a,*]

[a] *Instituto de Bioquímica Vegetal y Fotosíntesis, Universidad de Sevilla-Consejo Superior de Investigaciones Científicas, Centro de Investigaciones Científicas Isla de la Cartuja, Avda. Américo Vespucio, 49, 41092 Sevilla, Spain*

[b] *Department of Computer Science and Artificial Intelligence (University of Sevilla), Avenida Reina Mercedes s/n, 41012 Seville, Spain*

[c] *AlgaEnergy S.A, Avda. de Europa 19, 28108 Alcobendas, Madrid, Spain*

HIGHLIGHTS

- Massive metabolic reprogramming was unveiled for Haematoccocus reddish cells.
- The differential expression of 100s of genes induces this metabolic reprogramming.
- bHLH transcription factor family is a putative astaxanthin biosynthesis regulator.
- Vegetative reddish palmelloid cells are a model for astaxanthin synthesis studies.

GRAPHICAL ABSTRACT

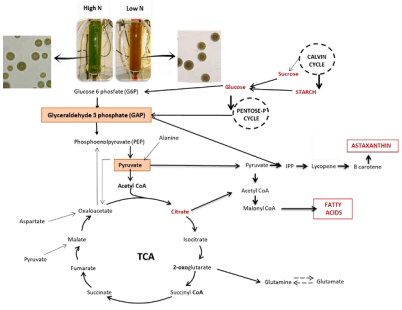

Keywords:

Astaxanthin

Carotenogenesis

H. pluvialis

Transcriptome sequencing

Metabolic pathways

ABSTRACT

Astaxanthin is a valuable and highly demanded ketocarotenoid pigment, for which the chlorophycean microalga *Haematococcus pluvialis* is an outstanding natural source. Although information on astaxanthin accumulation in *H. pluvialis* has substantially advanced in recent years, its underlying molecular bases remain elusive. An integrative metabolic and transcriptomic analysis has been performed for vegetative *Haematococcus* cells, grown both under N sufficiency (green palmelloid cells) and under moderate N limitation, allowing concurrent active cell growth and astaxanthin synthesis (reddish palmelloid cells). Transcriptional activation was noticeable in reddish cells of key enzymes participating in glycolysis, pentose phosphate cycle and pyruvate metabolism, determining the adequate provision of glyceraldehyde 3 phosphate and pyruvate, precursors of carotenoids and fatty acids. Moreover, for the first time, transcriptional regulators potentially involved in controlling astaxanthin accumulation have been identified, a knowledge enabling optimization of commercial astaxanthin production by *Haematococcus* through systems metabolic engineering.

* Corresponding author.
E-mail address: mggonza@us.es (M. García-González).

[1] Cristina Hoys and Ana B. Romero-Losada have contributed equally to this work.

1. Introduction

Astaxanthin, a most valuable carotenoid pigment, has found use as a potent natural antioxidant, nutraceutical, safe colouring agent in the food and health sectors, as well as a feed additive in aquaculture and poultry industries (Guerin et al., 2003).

The unicellular freshwater microalga *Haematococcus* is recognized as a rich natural resource of this ketocarotenoid, having the ability to accumulate in resting haematocysts up to 4% astaxanthin on a per dry weight basis (Del Río et al., 2010). Although this microalga has a complex and not well-defined life cycle, a consensus exists regarding its main morphotypes. In its vegetative (growing and dividing) stage, both motile (flagellated) and non-motile (palmelloid) cells can be found. Green cells predominate under favourable conditions of moderate irradiance and nutrients availability, whereas differentiation to the red resting form (haematocyst) is observed under stress conditions, including N and phosphate depletion, high light irradiance and salinity, high organic C/N ratio in nutrients supply and abundance of reactive oxygen species. Haematocysts are bigger in size than other morphotypes and are characterized by a thick cell wall and a massive accumulation of astaxanthin that is assumed to be linked to cessation of growth (Fábregas et al., 2001). Nevertheless, astaxanthin accumulation has also been described to take place in vegetative morphotypes (Del Río et al., 2005; Fang et al., 2020). In this context, Fang et al. (2020) have proposed the non-motile cell as a most appropriate cell type for astaxanthin photoinduction.

In *Haematococcus,* astaxanthin accumulation occurs in extra-plastidic globules, associated with fatty acids, and follows the general carotenoid pathway up to β-carotene formation (Grünewald et al., 2001). There is evidence for the operation of the full set of enzymes required for the conversion of pyruvate and glyceraldehyde 3—phosphate (GAP) into isopentenyl pyrophosphate (IPP) through the MEP (methyleritrol phosphate) pathway (Gwak et al., 2014). According to Shah et al (2016), approximately 10% of the biomass of *Haematococcus* cells in the green stage, consisted of fatty acids (FA), mostly C16 and C18, organized into small lipid bodies (LB). Under stress conditions, triacylglycerol (TAG) content and the number and size of LB increased in parallel to astaxanthin deposition. Indeed, astaxanthin synthesis in *Haematococcus* has been directly correlated in space and time with deposition of cellular reserves in LB under stress conditions (Solovchenko, 2015). Additionally, inhibition of de novo FA biosynthesis resulted in a severe decrease of astaxanthin biosynthesis, supporting the coupling between both process in *Haematococcus* (Chen et al., 2015).

Transcriptome sequencing represents a valuable approach for exploring the mechanism of astaxanthin accumulation. Changes in the expression of carotenogenic genes have been discussed in several studies, e.g. they were shown to be up regulated by high light (Römer and Fraser, 2005) or a combination of light and N starvation (Grünewald et al., 2001). Improvement of astaxanthin accumulation by gibberellin was accompanied by increased transcription of *IPI*, *PSY*, *PDS* and *BKT* genes (Gao et al., 2013).

Considerable efforts have focused on understanding the regulation of carotenogenic genes involved in astaxanthin biosynthesis. Nevertheless, most of these studies (Recht et al., 2014; Wase et al., 2014) have been carried out using batch systems, and involving severe stress conditions. The transformation of vegetative cell forms into haematocysts taking place in these situations involve dramatic morphological and metabolic changes. Such massive differences between reference morphotypes hamper the determination of the changes specifically related to astaxanthin metabolism. This makes imperative the introduction of new alternative *Haematococcus* cell models in which the conditions inducing astaxanthin accumulation do not produce complex side structural and/or metabolic changes with respect to the control cells, in which astaxanthin synthesis proceeds at a minimum or not at all. The availability of such alternative model systems would undoubtedly facilitate approaches to unveil the regulatory mechanisms underpinning astaxanthin accumulation in *Haematococcus*.

The continuous culture approach has demonstrated its suitability for the precise identification of nutritional and environmental factors influencing the accumulation of astaxanthin in *H. pluvialis* (Del Río et al., 2005; García-Malea et al., 2009). In these systems, the effect of each individual variable influencing performance of the culture can be specifically analysed while keeping all other growth parameters constant. Such continuous systems represent ideal experimental frameworks for transcriptomic and metabolomic studies that require fully reproducible, reliable, and biologically homogeneous data (Hoskisson and Hobbs, 2005).

A model *Haematococcus* cell system has been carefully designed for the present work. It consists of reddish cells raised in continuous culture under moderate nitrate limitation (2 mM nitrate in feed medium), able to develop at a high specific growth rate (0.8 d^{-1}) and accumulate astaxanthin simultaneously. The reference for comparison consists of green cells raised under analogous conditions, differing only in the nitrate supply (15 mM in the feed medium). In this work, such model system has been applied to search for a more comprehensive system view of the carotenogenic process, through an integrative metabolomic and transcriptomic study, involving the comparison of reddish and green *Haematococcus* cells. Specifically, our analyses aim at unveiling the molecular mechanisms controlling astaxanthin biosynthesis and accumulation in *Haematococcus*. In addition, related metabolic pathways as FA biosynthesis, starch accumulation, citric acid cycle and pentose phosphate cycle have also been examined, aiming to achieve a deeper understanding of the molecular mechanisms underpinning astaxanthin accumulation in *Haematococcus*. This knowledge, being highly valuable from the basic viewpoint, could also have practical implications in facilitating optimization of commercial astaxanthin production by this microalga.

2. Materials and methods

2.1. Organism and culture conditions

The microalga *Haematococcus pluvialis* (strain CCAP 34/8, formerly listed as *Haematococcus lacustris*, syn) was from Culture Collection of Algae and Protozoa of the Centre for Hydrology and Ecology, Ambleside, UK. Cells were grown photoautotrophically in jacketed bubble columns (0.06 m diameter, 0.50 m height), containing 1.8 L of cell suspension. The photobioreactors were continuously sparged with air (12 L/h). Temperature was maintained at 25 °C by flowing thermostat water through the photobioreactor jacket. The pH was kept close to 7 by on-demand injection of pure CO_2 into the air stream entering the culture. Each photobioreactor was illuminated by six surrounding Phillips Master TL5HO 24 W/840 white-light lamps in a simulated solar cycle mimicking natural outdoor conditions (12 h light/12 h dark), with irradiance increasing progressively to reach a maximum impinging on the reactor surface of 2000 μE m^{-2} s^{-1} at the sixth hour of the light period, to decrease progressively thereafter for additional 6 h until reaching the dark period. Cultures were carried out in continuous mode, at a dilution rate of 0.8 day^{-1}. The basal inorganic culture medium used to feed the reactor was as previously described (Del Río et al., 2005). The feed medium contained sodium nitrate at the concentration indicated, either 15 mM (N sufficiency, palmelloid green cells) or 2 mM (moderate N limitation, palmelloid reddish cells). For each treatment, four independent repeats were analysed. No analytical determination in the cells was performed until the cultures reached a stable steady-state situation. Statistical analysis of the data was carried out using t-student test with $p < 0.05$. Samples were always collected 6 h after the beginning of the light period.

2.2. Analytical procedures

Samples of the culture suspensions were collected following a

quenching approach (Veyel et al., 2014), 6 h after initiation of the illumination period. For this, 100 mL culture aliquots were cold centrifuged quickly (1 min 3500xg). The pellet was washed with the same volume of distilled water, centrifuged again under the same conditions, and the washed cells pellet frozen in liquid N and lyophilized (Skadi-Europe TFD 8503). The lyophilized biomass was flushed with N stream to prevent oxidation and stored at − 20 °C.

Carotenoids in biomass were determined in acetone extracts from 20 mg of lyophilized biomass, employing mechanical disruption with 2.7 mm glass beads in a Mini Bead Beater (Biospec Products), using HPLC-chromatography, as described in Del Campo et al. (2004).

Fatty acid content (% DW) and profile (% of total FA) were analysed by gas chromatography, according to Del Río et al. (2015).

The methodology described in García-Cubero et al. (2018) was used to determine *starch* content from 5 mg lyophilized samples in 1 mL of chloroform:methanol solution (2:1 v/v).

Determination of *free amino acids* content was carried out by high performance liquid chromatography (HPLC, Hitachi Ellite Lachrom), using a C18 column (LichroCART® 125–4, Merck) in reverse phase of 125 mm in length, with 5 μm of particle size, 125 Å pore size and 3 mm internal diameter. For the preparation of the extract, 0.4 mL of 0.1 N HCl was added to 20 mg of lyophilized biomass. After incubation on ice for 1 h, the extract was derivatized with phenyl isothiocyanate following the protocol described by (Heinrikson and Meredith, 1984). Absorbance detection was carried out at 254 nm. For calibration, standards composed of a commercial mixture of amino acids (AAS18 Sigma – Aldrich, St. Louis, USA) was supplemented with asparagine, glutamine and tryptophan (Sigma-Aldrich, St. Louis, USA) which are added to the mixture dissolved in HCl (0.1 N).

For *organic acids and sugars* analysis, GC/MS was carried out according to Veyel et al. (2014). 20 mg of lyophilized biomass were subjected to mechanical breakage with glass beads of 2.7 mm in Mini Bead Beater, using as solvent 3 mL of a mixture of methanol:chloroform:water (5:2:1) with 5 μL of 4 mM ribitol (prepared in methanol) as internal standard. Following centrifugation, the pellet was washed until the supernatant was colourless. The combined supernatants were dried under N stream and stored at − 20 °C until derivatization and subsequent analysis. For derivatization, dried samples were resuspended in 0.1 mL of pyridine, supplemented with 0.2 mL methoxyamine and incubated for 90 min in a thermostat shaker at 37 °C. Thereafter, 0.2 mL of N-Methyl-N-(trimethylsilyl)-trifluoroacetamide (MSTFA) was added and incubated for 30 min at 37 °C with continuous shaking (Roessner et al., 2001). Separation and quantification of organic acids were carried out in quadruple GCMS-QP2010 Plus (Shimadzu, Kyoto, Japan) with a capillary column MetaX5 (30 m, 0.25 mm, 0.25 μm) with simultaneous SIM and full scan acquisition mode. For sugars, a capillary column VF – 1 ms (25 m; 0.20 mm; 0.33 μm; Agilent Technologies) was used, in the SIM acquisition mode. For the qualitative analysis, the CGMS Solution 2.30 software mass spectra was used, comparing the obtained retention times and mass spectra with the Wiley 229 and NIST11 libraries. Quantification was performed on the basis of calibrated peak areas for commercial standards normalized in relation to that of ribitol.

2.3. Electron microscopy

For cell fixation, 1 mL of fresh culture was centrifuged (1 min, 12,100 xg). After washing with ammonium formiate (1%), the pellet was treated with 1 mL of glutaraldehyde 2.5% in cacodylate buffer (0.1 M, pH 7.38) by incubating at 4 °C with shaking for 2 h, performing 5 washes with the same buffer. For inclusion in the resin, the fixed cells were washed again with cacodylate buffer for 15 min at 4 °C (3 times). They were incubated with osmium tetroxide 1% 1 h at 4 °C followed by 3 washes with distilled water and incubated with 2% uranyl, 2 h at 25 °C. The samples were dehydrated with acetone solutions in a gradient of 50%, 70%, 90% (30 min, 25° C) and 100% (2 sequential incubations of 20 min at 25 °C). Subsequently, three consecutive incubations of 2 min were carried out at 25° C using acetone: resin in proportions 3:1, 1:1 and 1:3, respectively. Finally, cells were embedded in 100% resin and incubated at 25° C for 15 min. To obtain ultra-fine sections (50–70 nm) an ultra-microtome Leica UC7 (Leica Microsystems) was used and visualized in an electron microscope of transmission (Libra 120 Plus; Zeiss Iberia).

2.4. RNA-seq data generation and processing

Total RNA was extracted using TRIsure™ following manufacturer's instructions. Subsequently, RNA was purified using ISOLATE II RNA Plant Kit attending manufacturer's instructions. Sequencing libraries were generated according to Illumina TruSeq Stranded mRNA protocol. Libraries were sequenced on an Illumina NextSeq 500 sequencer producing approximately 20 million 75nt long single end reads per sample. The software package FASTQC (https://www.bioinformatics.babraham.ac.uk/projects/fastqc/) was used to perform quality control of the sequencing raw data. The draft genome sequence assembly v1.0 and annotation of *Haematococcus lacustris* (accession number GCA_011766145.1) were used as reference genome (Morimoto et al., 2020). The software tools HISAT2 (Kim et al., 2019) and StringTie2 (Kovaka et al., 2019) were used for read mapping to the reference genome, transcripts assembly and gene expression estimation as FPKM (Fragments Per Kilo base per million Mapped reads) using default parameters. De novo transcript assembly of unmapped reads was carried using Trinity (Haas et al., 2013). Transdecoder was used to identify complete ORFs in the corresponding transcript sequences.

2.5. Transcriptomic data analysis and functional enrichment

The Bioconductor R package ballgown was used to import RNA-seq processed data (Frazee et al., 2015). Differentially expressed genes were determined with the Bioconductor R package limma (Ritchie et al., 2015) according to a log2FC of ± 1 and a q-value or FDR threshold of 0.05. To perform functional enrichment analysis, an R annotation data package for *Haematococcus lacustris org.Hlacustris.eg.db,* was developed freely available from the GitHub repository: https://github.com/ABRomeroLosada/tartessos_RNAseq. PFAM (protein family), GO (Gene Ontology) and KO (KEEG orthology) annotations were assigned to each *Haematococcus* gene, including de novo assembled and newly identified transcripts, using HMMER3 (Mistry et al., 2013), pfam2go mapping (http://current.geneontology.org/ontology/external2go/pfam2go) and KEGG Automatic Annotation Server (KAAS) (Moriya et al., 2007) respectively. GO and KEGG pathways enrichment analysis over the set of differentially expressed genes were performed using the bioconductor R package clusterProfiler (Yu et al., 2012).

2.6. Transcription factors identification and DNA motifs enrichment analysis

The genome wide identification of transcription factors in *Haematococcus* was performed following the characterization presented in PlantTFDB (Jin et al., 2017) using our PFAM annotation. For the purpose of performing DNA motifs enrichment analysis, an R transcript annotation package for *Haematococcus lacustris TxDb.Hlacustris.NCBI* was developed and freely available from the GitHub repository: https://github.com/ABRomeroLosada/tartessos_RNAseq.

Gene promoters were defined as the region 1 Kb upstream from coding sequences start points. The software tools MEME and TomTom (Bailey et al., 2009) were used to identify DNA motifs in the promoters of the different gene sets and to compare them against the *Arabidopsis thaliana* TFBS (transcription factor binding sites) databases DAP motifs (O'Malley et al., 2016) and PBS motifs (Franco-Zorrilla et al., 2014).

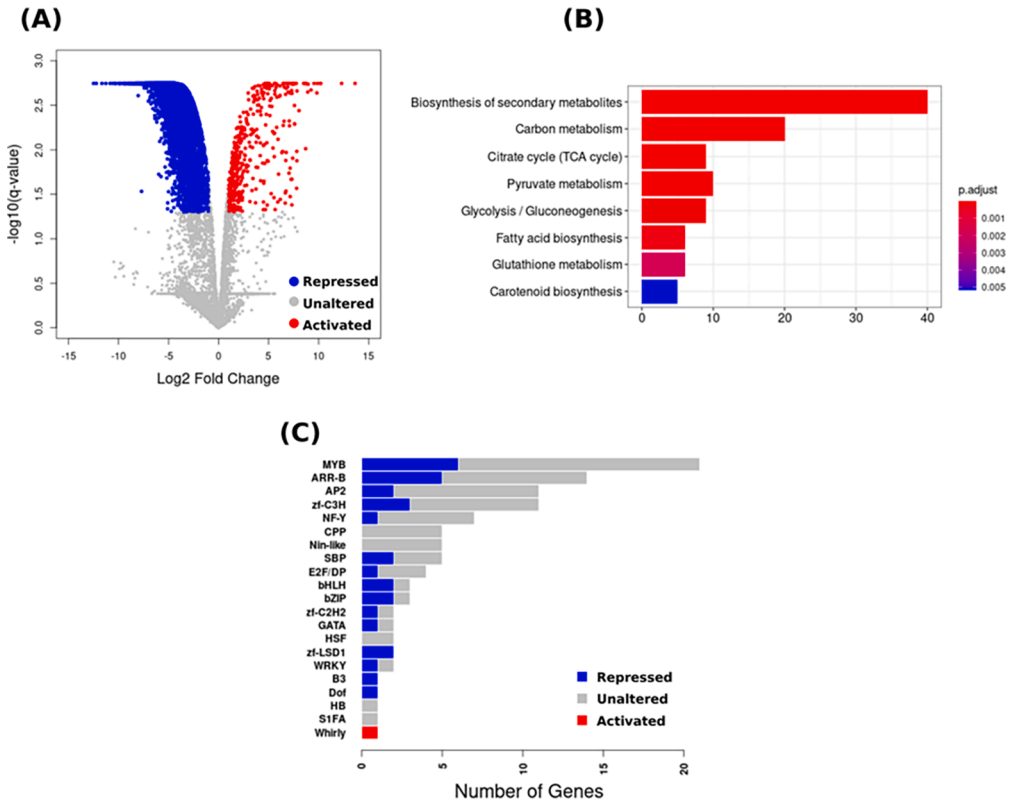

Fig. 1. Differential gene expression in reddish *Haematococcus* cells (grown under moderate N limitation) as compared to green cells (grown under N sufficiency). (A) Volcano plot representing differentially expressed genes. Each dot represents a gene where its x and y coordinates stand for its log2 fold change and its significance level, respectively. (B) Bar plot depicting significantly enriched biological pathways among the activated genes. Bar length represents the number of activated genes associated to each pathway. A color gradient from blue to red is used to represent low to high significance levels. (C) Bar plot showing the number of repressed, unaltered and activated genes codifying transcription factors from different families. Bar length represents the number of genes. (For interpretation of the references to color in this figure legend, the reader is referred to the web version of this article.)

3. Results and discussion

The main objective of the current study was to gain understanding of the molecular mechanisms underlying astaxanthin accumulation in actively growing cells of the chlorophycean microalgae *Haematococcus,* mainly through the combined analysis of metabolite and gene expression profiles. To this end, two distinct cell populations grown in continuous culture were compared: i) reddish palmelloid cells, raised in cultures fed with fresh medium containing 2 mM nitrate (moderate N limitation) maintaining a stable biomass concentration of 0.8 g l^{-1}, with astaxanthin and N content of 0.21% and 5%, respectively, and a C/N ratio of 10; and ii) green palmelloid cells raised in continuous cultures containing 15 mM nitrate in the feed medium, with stable biomass concentration of 0.9 g l^{-1} and astaxanthin and N content of 0.014% and 8%, respectively, and a C/N ratio of 6. See graphical abstract.

3.1. Transcriptomic reprogramming under astaxanthin accumulation conditions

To learn about transcriptomics of astaxanthin accumulation, we performed genome-wide expression profiling, using RNA-seq for both reddish and green *Haematococcus* cells. Initially, less than half of the reads mapped to the reference draft genome, which has been estimated to be only 57.7% complete (Morimoto et al., 2020). To improve its extensiveness, transcripts were de novo assembled using only the unmapped reads and included in the reference genome. This resulted in the assembly of 518 transcripts containing complete coding sequences with significant identification of protein domains or exhibiting significant

Table 1
Significantly activated molecular pathways in reddish *Haematococcus* cells (grown under moderate N limitation) as compared with green cells (grown under N sufficiency).

Pathway Description	Enrichment*	FDR**	Gene
Biosynthesis of secondary metabolites	2.43	1.19×10^{-7}	*CYP51* (HaLaN_02928) *GMPP* (HaLaN_00093)
Carbon metabolism	4.13	3.33×10^{-7}	*G6PDH* (HaLaN_06758) *PGD* (HaLaN_11988)
Citrate cycle (TCA cycle)	7.43	1.26×10^{-5}	*SCL* (HaLaN_17954) *IDH* (HaLaN_22540)
Pyruvate metabolism	6.35	1.35×10^{-5}	*PDHA1* (HaLaN_05256) *PK* (HaLaN_06731)
Glycolysis / Gluconeogenesis	6.19	5.34×10^{-5}	*PCK* (HaLaN_13453) *GAPDH* (HaLaN_25066)
Fatty acid biosynthesis	9.01	1.55×10^{-4}	*ACACA* (HaLaN_08198) *SSI2* (HaLaN_23803)
Glutathione metabolism	6.19	1.47×10^{-3}	*GST* (HaLaN_22187) *SRM* (HaLaN_11658)
Carotenoid biosynthesis	6.35	4.17×10^{-3}	*LCY-β* (HaLaN_05151) *BKT* (HaLaN_04875)

*Over-representation with respect to the random expected value.
** False Discovery Rate.

Table 2
Carotenoid content of reddish *Haematococcus* cells (grown under moderate N limitation) and green cells (grown under N sufficiency).

Carotenoid (mg/g dry biomass)	Green cells	Reddish cells
α-carotene	0.03 ± 0.00	n.d.*
lutein	1.29 ± 0.01	0.71 ± 0.03
β-carotene	0.50 ± 0.04	0.22 ± 0.01
canthaxanthin	0.01 ± 0.00	0.09 ± 0.02
violaxanthin	0.45 ± 0.04	0.27 ± 0.02
astaxanthin	0.14 ± 0.02	2.08 ± 0.36

*No detectable.

sequence similarity with previously annotated protein sequences in the green lineage. After this improvement of the current draft genome sequence, the mapping rate for each sample was greater than 86%. The integration of our RNA-seq data into the current draft genome would improve the gene annotation as well as the identification of new unannotated genes.

The criterion for differentially expressed genes was established on the basis of differences in gene expression, either increase or decrease, greater than two-fold with a q-value or FDR (False Discovery Rate) < 0.05. A major transcriptional reprogramming was evident in reddish cells compared to the green ones, Fig. 1. Specifically, 414 differentially activated genes were found. Pathway enrichment analysis was performed over this gene set aiming to identify the metabolic processes associated to astaxanthin synthesis and accumulation, Fig. 1. Central metabolic pathways, such as biosynthesis of secondary metabolites, pyruvate metabolism, FA and carotenoid biosynthesis, were found to be significantly affected, Table 1.

Differentially expressed transcription factors were also identified in a search for potential regulators of the corresponding activated biological processes. As much as 104 genes codifying for transcription factors belonging to 21 different protein families in the current *Haematococcus* draft genome sequence were found. Around a third of them, 31 transcription factors, were significantly repressed in reddish cells, Fig. 1. This suggests that part or all the recorded activations could arise from a derepression process, in which removal of a repressor resulted in the activation of its target gene, rather than from a direct activation. Only one transcription factor from the Whirly family was found to be significantly activated, Fig. 1. In what follows, the transcriptomic results were integrated with those obtained for cellular content of key metabolites in the significantly affected metabolic pathways, to perform a systemic characterization of molecular changes linked to astaxanthin accumulation in *Haematococcus*.

3.2. Activation through derepression of key carotenogenic genes probably involves participation of bHLH transcription factors

Carotenoid biosynthesis was identified as one of the significantly activated metabolic pathway in our transcriptomic analysis, Table 1. Actually, the values for carotenoid and astaxanthin content in reddish cells were 1.4-fold and 15-fold higher, respectively, than those in green cells, Table 2.

Genes codifying for all the enzymes involved in astaxanthin biosynthesis were identified in the current draft genome sequence and differences in gene expression between reddish and green cells were computed Table 3. The transcriptomic analysis identified in reddish cells higher expression of all genes involved in the MEP (non-mevalonate) pathway, only expressed at a basal level in green cells. In parallel, expression of all genes related to astaxanthin biosynthesis was also higher in reddish than in green cells. Fig. 2 shows, in a graphical way, the relative expression ratio between reddish and green cells for the different genes, as well as the content of relevant metabolites in both cell types.

Starting with the MEP pathway, we found activation in reddish cells of the key genes *IPI1/2,* Fig. 2, Table 3. These genes encode IPI, involved

Table 3
Expression ratio between reddish and green cells of genes codifying for enzymes involved in different metabolic pathways in the *Haematococcus* genome.

Enzyme Name	Symbol	Gene ID	Fold-change[a]
Carotenoid Biosynthesis			
1-hydroxy-2-methyl-2-(E)-butenyl-4-diphosphate reductase	HDR	HaLaN_06917	3.7
isopentenyl pyrophosphate isomerase	IPI	HaLaN_15304	1.99
geranylgeranyl diphosphate synthase	GGPS	HaLaN_05222	2.51
phytoene synthase	PSY	HaLaN_19207	4.92
phytoene desaturase	PDS	HaLaN_01499	5.18
zeta-carotene desaturase	ZDS	HaLaN_15035	5.01
lycopene β-cyclase	LCYB	HaLaN_05151	7.81
β-carotene ketolase	BKT	HaLaN_04875	11.72
β-carotene hydroxylase	CHYB	HaLaN_14026	2.89
Lycopene ε-cyclase	LCYE	HaLaN_15758	0.05
β-ring hydroxylase	BCHB	HaLaN_29254	0
zeaxanthin epoxidase	ZEP	HaLaN_17766	1.68
violaxanthin de-epoxidase	VDE	HaLaN_22693	0
Fatty Acids Biosynthesis			
pyruvate kinase	PK	HaLaN_06731	3.07
phosphoenolpyruvate carboxylase	PEPC	HaLaN_29239	1.98
phosphoenolpyruvate carboxykinase	PEPCK	HaLaN_13453	30
pyruvate dehydrogenase E1 component alpha subunit	PDHE1a	HaLaN_05256	5.64
pyruvate dehydrogenase E1 component beta subunit	PDHE1b	HaLaN_03083	4.58
pyruvate dehydrogenase E2 component	PDHE2	HaLaN_06535	4.05
acetyl-CoA carboxylase, biotin carboxylase subunit	ACCBC	HaLaN_04167	3.53
acetyl-CoA carboxylase carboxyl transferase subunit alpha	ACACA	HaLaN_08198	3.63
acetyl-CoA carboxylase carboxyl transferase subunit beta	ACACB	HaLaN_00479	3.49
malonyl-CoA-acyl carrier protein transacylase	MCAT	HaLaN_32744	3.37
3-ketoacyl-ACP synthase II	KASII	HaLaN_03364*	3.44
3-ketoacyl-ACP synthase III	KASIII	HaLaN_25691	2.35
3-ketoacyl-ACP reductase	KAR	HaLaN_16400	3.24
long-chain acyl-CoA synthetase	LACS	HaLaN_18308	1.06
stearoyl-ACP-desaturase	SAD	HaLaN_23803	4.38
Starch and Sugar Metabolism			
ADP glucose pyrophosphorylase Large Subunit	APL	HaLaN_18631	0.76
Soluble Starch Synthase	SSS	HaLaN_03235	2.15
Disproportionating Enzyme	DPE	HaLaN_18482	1.88
Glycogen phosphorylase	GLGP	HaLaN_16242	2.05
Granule Bound Starch Synthase	GBSS	HaLaN_12479	2.02
Starch Branching Enzyme	SBE	HaLaN_06055	1.52
Trehalose 6-phosphate synthase/phosphatase	TPS	HaLaN_05935	0
Glyceraldehyde 3P dehydrogenase	GAPDH	HaLaN_27953	15.13
Glucose 6P Dehydrogenase	G6PDH	HaLaN_06758	4.08
6P Gluconate Dehydrogenase	6PGDH	HaLaN_11988	4.04
Nitrogen Assimilation and Metabolism			
Nitrate/nitrite Transporter	NRT	HaLaN_08568	3.47
Nitrate Reductase	NR	HaLaN_08567	1.87
Glutamine Synthetase	GS	HaLaN_07426	1.62
Glutamate Synthase	GOGAT	HaLaN_08200	0.95
Aspartate Aminotransferase	AAT	HaLaN_06291	4.63
Alanine Aminotransferase	ALT	HaLaN_04431	1.26
TCA cycle			
Citrate Synthase	CS	HaLaN_15872	1.70
Aconitase	ACO	HaLaN_27844	1.68
Isocitrate Dehydrogenase	IDH	HaLaN_0276	2.43
2-oxoglutarate Dehydrogenase	OGDH	HaLaN_08192	2.83
Succinyl-CoA synthetase alpha subunit	SUCA	HaLaN_17954	2.26
Succinyl-CoA synthetase beta subunit	SUCB	HaLaN_30125	2.60
Succinate Dehydrogenase	SDH	HaLaN_29098	0.54
Fumarase	FUM	HaLaN_08385	22.16
Malate Dehydrogenase	MDH	HaLaN_00470	0.93

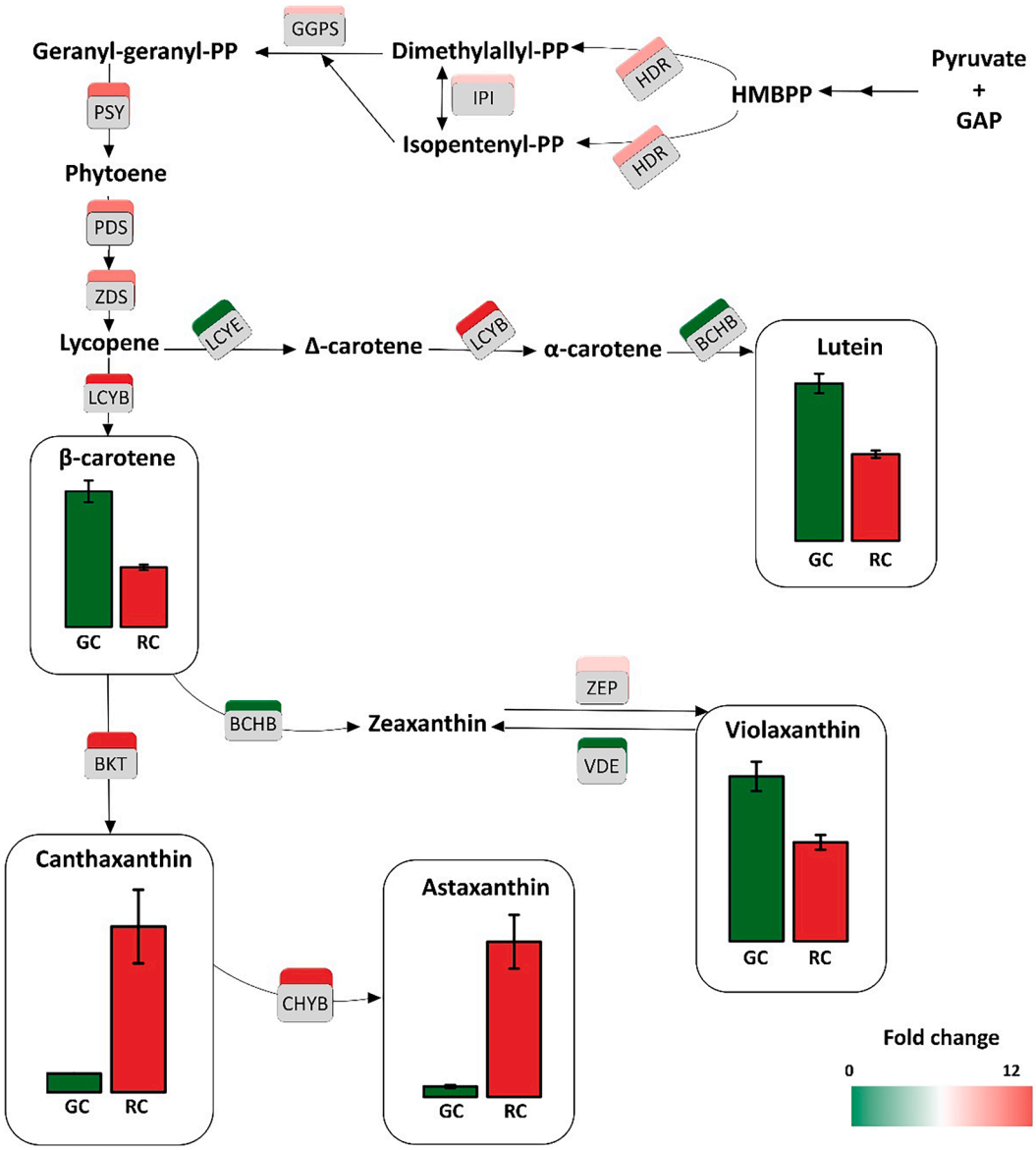

Fig. 2. Differential expression of genes involved in the astaxanthin biosynthesis pathway and cellular content of carotenoids in reddish (RC) and green (GC) *Haematococcus* cells. A colour gradient from green to red (0–12) is used to represent the fold-change in gene expression of reddish in comparison to green cells. The full name of the enzymes corresponding to each abbreviation is in the text. (For interpretation of the references to color in this figure legend, the reader is referred to the web version of this article.)

in the interconversion between IPP and dimethylallyl diphosphate (DMAPP). This, together with the activation of genes encoding 1-hydroxy-2-methyl-2-(ε)-butenyl-4-diphosphate reductase (HDR) and geranylgeranyl pyrophosphate synthase (GPPS), could sustain the biosynthesis of adequate upstream intermediates for carotenoid biosynthesis. These results contrast with previous information indicating that none of the two *IPI* gene was up regulated in the case of astaxanthin accumulation induced by high irradiance and suggested that 4-hidroxy-3-methylbut-2-enyl diphosphate reductase (ISPH) was responsible to the interconversion between IPP and DMAPP (Gwak et al., 2014).

Regarding the synthesis of phytoene and lycopene, catalysed by phytoene synthase (PSY), phytoene desaturases (PDS) and the recently identified ξ-carotene desaturase (ZDS) (Lee et al., 2016), the genes encoding the three enzymes exhibited a higher expression in reddish cells, Fig. 2, Table 3, indicating preferential funnelling of carbon skeletons into astaxanthin biosynthesis.

Downstream from lycopene, a clear upregulation of the carotenoid biosynthesis β-branch, in parallel with repression of the ε-branch and xanthophyll cycle, was apparent for reddish as compared to green cells. A particularly pronounced activation was found for lycopene β-cyclase (LCYB), whereas lycopene ε-cyclase (LCYE) and β-ring hydroxylase (BCHB) were severely repressed. This resulted in a decreased competition for lycopene between lutein synthesis and that of β-carotene, precursor of the xanthophyll cycle. Consequently, reddish cells presented lower lutein and violaxanthin content, by 1.8 and 1.7-fold, respectively, than those in green cells, Fig. 2. These results are in agreement with previous transcriptomic data (Fang et al., 2020; Gao et al., 2015; He et al., 2018) obtained under different stress conditions. Following the β-branch, higher expression of β β-carotene ketolase (BKT) and β β-carotene hydroxylase (CHYB) was detected in correspondence with 9 and 15-fold higher canthaxanthin and astaxanthin content, respectively, in reddish cells. The oxygenations catalysed by these enzymes are regarded as rate limiting steps of astaxanthin synthesis in *Haematococcus* (Fang et al., 2020).

Again, this agrees with results reported for *Haematococcus* subjected

to other astaxanthin accumulation conditions such as high light (Gwak et al., 2014), sodium acetate (Vidhyavathi et al., 2008), disodium 2-oxoglutarate (Lu et al., 2020), ethanol (Wen et al., 2015) or salicylic acid and jasmonic acid (Gao et al., 2015), when comparing green cells with haematocysts. This reinforces the view of a common transcriptomic response affecting the conversion of lycopene into the different xanthophylls, regardless the conditions applied to promote astaxanthin accumulation.

The concurrent activation recorded in genes codifying for enzymes involved in astaxanthin biosynthesis could indicate that they are co-regulated transcriptionally. To identify transcription factors that potentially coordinate the expression of these enzymes, we performed a DNA motif enrichment analysis over their promoter sequences. Three different DNA motifs were found to be present in the corresponding gene promoters, Fig. 3. The first and third more significative motifs presented a similarity to the consensus DNA sequence recognized in plants by transcription factors from the bZIP and bHLH families, respectively. In plants, carotenoids biosynthesis has been shown to be antagonistically regulated by a module comprising repression exerted by the bHLH factors PHYTOCHROME INTERACTING FACTORS (PIFs), and activation by the bZIP transcription factor ELONGATED HYPOCOTYL5 (HY5) (Toledo-Ortiz et al., 2014). Our analysis suggests that this regulatory transcriptional module could have been already established in Chlorophyta like *Haematococcus* and conserved during the entire green lineage evolution, leading to flowering plants. In agreement with this, all the bHLHs were found to be severely repressed in reddish cells, Fig. 3. Nonetheless, no bZIP transcription factor was found significantly activated, Fig. 2. This could indicate that de-repression of the corresponding bZIP factor suffices for the observed 15-fold higher astaxanthin level in reddish cells. The original identification of both, the potential transcriptional regulators and their binding sites, open up new avenues to genetic engineering approach, aimed at optimizing the commercial production of astaxanthin by *Haematococcus*.

Table 4
Fatty acid profile of reddish *Haematococcus* cells (grown under moderate N limitation) and green cells (grown under N sufficiency).

Fatty acid (% of total)	Green cells	Reddish cells
Myristic (C14:0)	0.08 ± 0.01	0.07 ± 0.01
Palmitic (C16:0)	17.52 ± 0.39	15.89 ± 1.27
Palmitoleic (C16:1)	2.25 ± 0.14	1.17 ± 0.04
Stearic (C18:0)	5.49 ± 0.35	4.94 ± 0.32
Oleic (C18:1)	15.81 ± 0.36	21.89 ± 2.33
Linoleic (C18:2)	13.03 ± 0.44	16.66 ± 0.68
Linolenic (C18:3n4)	20.60 ± 0.55	14.47 ± 0.44
Arachidonic (C20:6n4)	1.53 ± 0.12	1.37 ± 0.15

3.3. Orchestrated activation of key enzymes enhances availability of fatty acids for astaxanthin esterification

Fatty acid biosynthesis was also significantly activated in reddish cells, Table 1. To further explore and validate these results we quantified FA content in green and reddish cells, Table 4. In our continuous culture system, *H. pluvialis* palmelloid green cells exhibited a FA content of around 5% of the dry biomass. In palmelloid reddish cells, the FA content reached about 6.5%. The extra FA availability could satisfy the higher demand of FA for astaxanthin esterification in reddish cells. For *Haematococcus*, it has been described that about 90% of the astaxanthin molecules are esterified with FA being oleic (C18:1) the most common FA in these conjugates (Recht et al., 2014). The FA profile, Table 4, showed that, in green cells, linolenic (C18:3n4) was the predominant FA, representing over one fifth of total FA content. In the reddish cells, oleic (C18:1) was, however, the most abundant FA, reaching over 22% of total FA, i.e., 38% higher than that in green cells. To characterize the molecular mechanisms underpinning the observed differences in FA profile between the two types of cells, the expression of genes codifying for key enzymes involved in FA metabolism were analysed, Table 3. In Fig. 4, the FA biosynthetic pathway in *Haematococcus* is shown, with consideration of the expression ratio for genes codifying the key enzymes in reddish versus green cells, as well as their FA levels.

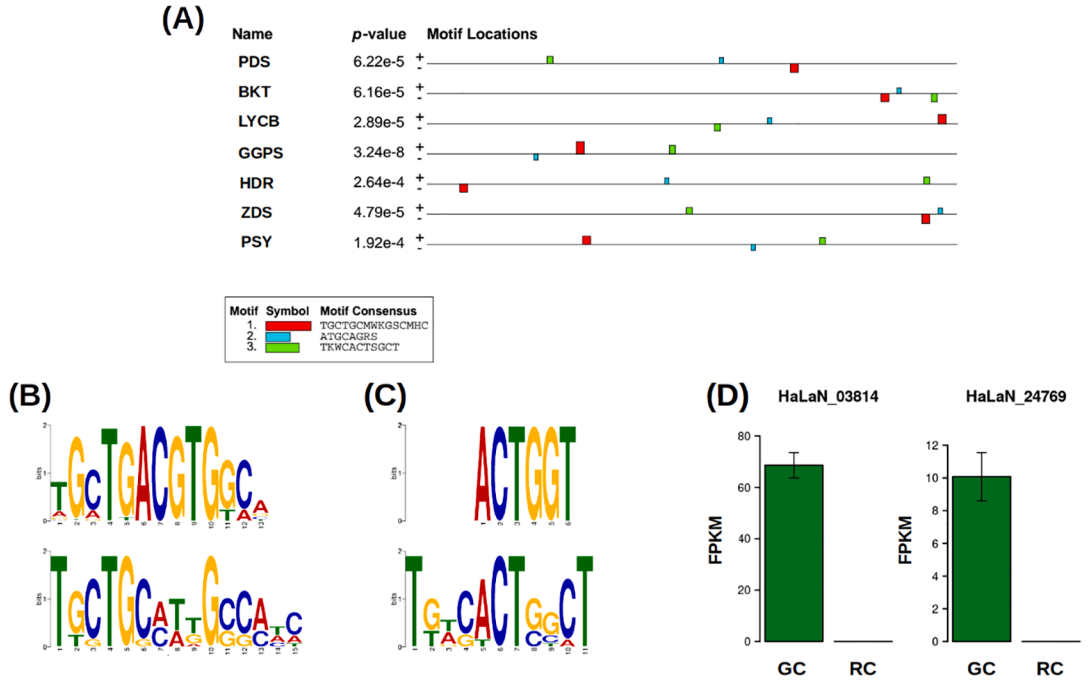

Fig. 3. DNA sequence analysis in reddish cells. (A) Identification of the prevalent DNA sequences in the promoters of key enzymes involved in astaxanthin biosynthesis in *Haematococcus* that are differentially activated in reddish cells. (B) Similarity between the prevalent sequence identified and a DNA motif recognised by bHLH transcription factors. (C) Similarity between the third prevalent sequence identified and a DNA motif recognised by bHLH transcription factors. (D) Expression bar plots showing the repression of the two bHLH transcription factors identified in the analysis, namely HaLaN_03814 and HaLaN_24769.

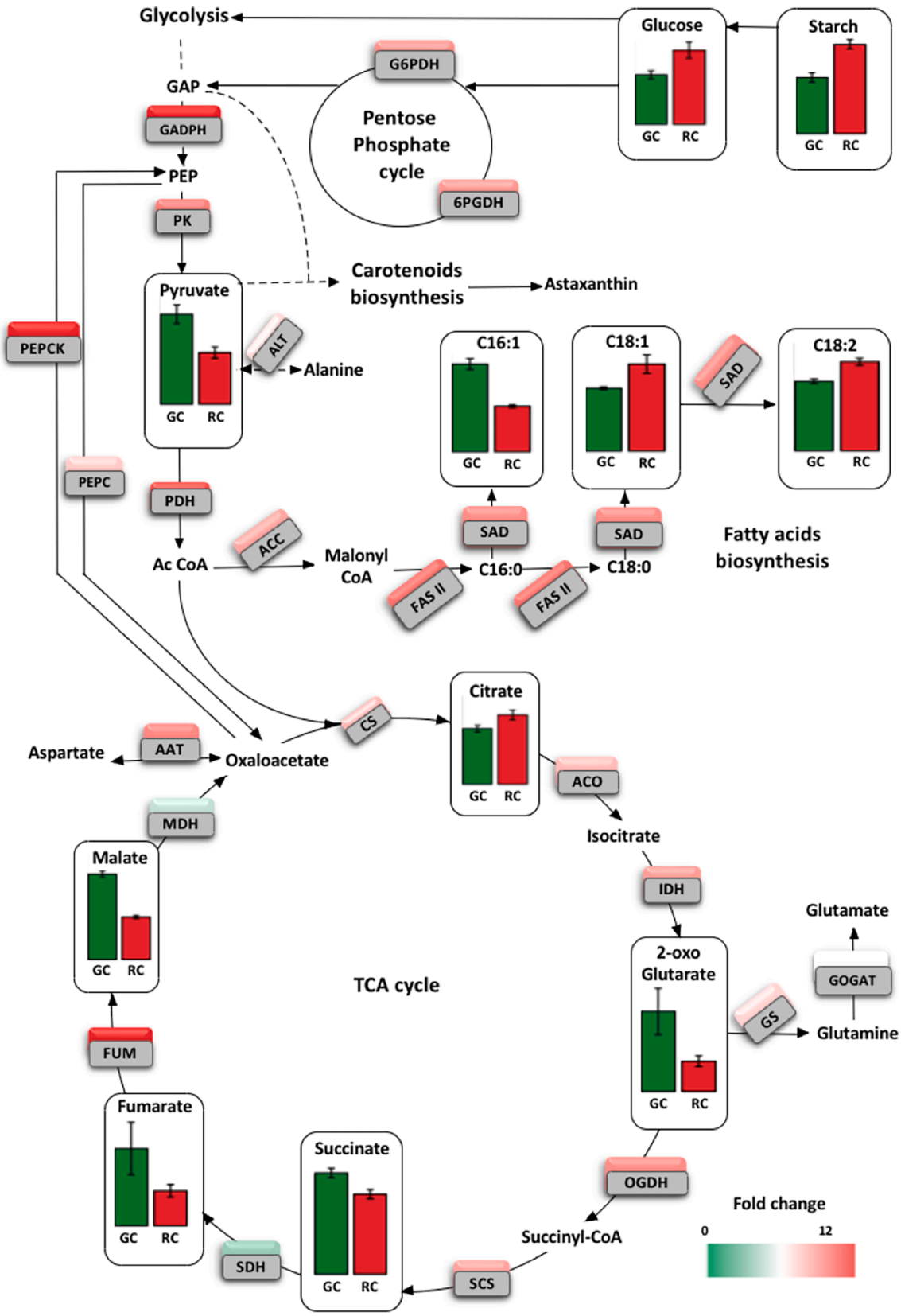

Fig. 4. Differential expression of genes involved in fatty acid synthesis, TCA cycle, glycolysis and starch degradation and cellular content of relevant metabolites in reddish (RC) and green (GC) *Haematococcus* cells. A colour gradient from green to red (0–12) is used to represent the fold-change in gene expression of reddish in comparison to green cells. (For interpretation of the references to color in this figure legend, the reader is referred to the web version of this article.)

Pyruvate metabolism, a significantly activated pathway in reddish cells, Table 1, has been described to play a major role in astaxanthin esterification (Chen et al., 2015). Pyruvate, the final product of glycolysis, can be further converted to IPP, precursor for astaxanthin synthesis, or to acetyl-CoA, to support FA biosynthesis. Pyruvate consumption by these two pathways could explain its detected 43% lower level in reddish cells with respect to green cells, Fig. 4. In the final step of glycolysis, pyruvate kinase (PK) catalyses the irreversible conversion of phosphoenolpyruvate (PEP) into pyruvate. *PK* gene expression was 3-fold higher in reddish cells. Regarding the conversion of pyruvate into acetyl-CoA by pyruvate dehydrogenase (PDH), expression of the genes codifying for the components of this complex was also high in reddish cells, Fig. 4, Table 3. Similar results have been reported for *Chlamydomonas reinhardtii* subjected to N stress (Wase et al., 2014). In reddish *Haematococcus* cells, no significant higher expression than in green cells of the gene codifying for malate dehydrogenase (MDH) was observed, but one of the two isoforms codifying for phosphoenolpyruvate carboxykinase (PEPCK) was indeed highly upregulated (30-fold), a situation leading to enhanced synthesis of PEP from oxaloacetate (OAA) that would result in additional availability of pyruvate for both, FA and astaxanthin production. Fang et al. (2020) have described the upregulation of MDH2 and PEPC enzymes in heterotrophically grown non-motile cells.

Acetyl-CoA is converted to malonyl-CoA, by acetyl-CoA carboxylase (ACC), a critical step in lipid biosynthesis. Expression of all the genes codifying for the different subunits of ACC was more than 3-fold higher in reddish than green cells. Activation of *ACC* would enhance the flux of C-2 precursors into FA biosynthesis (Huerlimann and Heimann, 2013). The malonyl-CoA:ACP (acyl carrier protein) transacylase (MAT) transfers a malonyl group forming malonyl-ACP to elongate the FA chain. One of the two isoforms found in the *Haematococcus* genome codifying for MAT exhibited higher expression (3-fold) in reddish than in green cells. The acyl-ACP chain is elongated throughout the seven activities of the fatty acid synthase type II (FASII) yielding C16:0 and C18:0. The genes codifying for the key catalytic components of FASII, 3-ketoacyl-ACP synthase II and III (KAS II and III), as well as 3-ketoacyl-ACP reductase (KAR) were highly activated in reddish cells when compared to green cells, Fig. 4, Table 3. Finally, a double bond must be introduced to the Δ9 position of C18:0 by stearoyl-ACP-desaturase (SAD) to form C18:1. One of the two isoforms codifying for SAD was strongly expressed in reddish cells, with over 4-fold higher level than in green cells. This would respond for the predominance of oleic acid (C18:1) in the FA profile of reddish cells, Fig. 4, which exhibited besides higher number and size of lipid bodies than the green cells.

Our integrative analysis provides a molecular mechanism for a favoured esterification of astaxanthin to be deposited in the LB of reddish cells, as well as for the concurrent biosynthesis of astaxanthin and FA.

3.4. Concurrent activation of key enzymes results in concomitant accumulation of starch granules and astaxanthin

More abundant and larger starch granules were observed in reddish than in green cells. This differential morphology was in line with the higher starch content in reddish cells, reaching 22% of the dry biomass, as compared to 13% for green cells, Table 5. Accordingly, although no significant difference was found between reddish and green cells in the expression level of the gene codifying for ADP glucose pyrophosphorylase (APL), higher expression was apparent in reddish cells for genes codifying other key enzymes in starch metabolism, such as soluble starch synthase (SSS), granule bound starch synthase (GBSS), starch branching enzyme (SBE), glycogen phosphorylase (GLGP) and disproportionating enzyme (DPE), Table 3. Although the process of starch granule initiation remains elusive, a central role of the three enzymes SSS, DPE and GLGP has been reported in the case of the model plant *Arabidopsis* (Malinova et al., 2017), with similar results being found for the microalga *Chlamydomonas reinhardtii* in response to N stress (Wase et al., 2014). Accumulation of carbohydrates has been described for *Haematococcus* cells as an early response to N starvation and high light, followed by FA accumulation (Recht et al., 2012), suggesting that the FA were, in part, built from starch degradation derivatives at the end of the stress response. Nevertheless, our results rather suggest that accumulation of FA and starch do occur simultaneously when astaxanthin biosynthesis proceed in the absence of severe stress conditions.

Table 5
Sugar profile of reddish *Haematococcus* cells (grown under moderate N limitation) and green cells (grown under N sufficiency).

Sugar (μmol sugar/g dry biomass)	Green cells	Reddish cells
Fructose	0.08 ± 0.02	0.12 ± 0.03
Galactose	1.94 ± 0.25	2.07 ± 0.41
Glucose	0.12 ± 0.01	0.18 ± 0.02
Sucrose	18.83 ± 3.08	66.52 ± 8.17
Trehalose	0.42 ± 0.05	0.25 ± 0.03
Starch	13.40 ± 0.89	22.23 ± 0.92

3.5. Sugar catabolism provides key intermediates for astaxanthin biosynthesis and accumulation

Photosynthetically generated sucrose can also be metabolized, via glycolysis, to yield pyruvate. Metabolomic analysis showed a 3.5-fold higher content in sucrose and 1.5-fold in glucose in reddish cells with respect to green cells, Table 5. This result could not be easily integrated in the gene expression analysis since no gene was found for sucrose synthase in the current draft *Haematococcus* genome sequence. CO_2 fixation did not appear to be modified in reddish cells, since the genes detected in relation to the Calvin cycle had analogous expression in both cell types. Nevertheless, higher expression of the gene for glyceraldehyde 3P dehydrogenase (GAPDH) occurred in reddish cells. This would allow enhanced pyruvate production. Both, GAP and pyruvate would be used in astaxanthin biosynthesis via the MEP pathway. Moreover, GAP is a precursor of glycerol 3P, which is required for the synthesis of TAG forming LB, wherein astaxanthin is accumulated. Expression of the genes for glucose 6P dehydrogenase (G6PDH) and 6P gluconate dehydrogenase (6PGDH) were 4-fold higher in reddish than in green cells. This suggests that the pentose phosphate pathway was up regulated in the reddish cells, resulting in an extra yield of GAP and pyruvate from glucose, Table 3. Furthermore, operation of both enzymes is also essential for appropriate generation of the NADPH required for the novo FA biosynthesis. Finally, we observed a 40% lower trehalose content in reddish cells that could be explained by strong repression of the gene codifying for trehalose 6-phosphate synthase/phosphatase (TPS).

A hypothetical metabolic regulation model for astaxanthin accumulation in high-light stressed *Haematococcus* was proposed by Lv et al. (2016) assigning a relevant role to the accumulation of GAP, pyruvate and 2-oxoglutarate, although these compounds were not detected by the authors. Our results support this view and extend it to the situation of astaxanthin accumulation under moderate N limitation.

3.6. Amino acid metabolism and nitrate assimilation are activated under conditions favouring astaxanthin accumulation

Lv et al. (2016) described higher amino acids content for *Haematococcus* cells stressed by high light reaching the "yellow phase". However, Hu et al. (2020) reported a lower content under the same stress condition. In our work, levels of the different amino acid in reddish cells accumulating astaxanthin were significantly lower than in green cells, Table 3. It has been reported that the content of amino acids in stressed yeasts is directly related to that of their metabolic precursors (Rodrigues-Pousada et al., 2004). For instance, GAP is a precursor of serine and threonine, and pyruvate is a precursor of leucine, isoleucine, valine and alanine. According to our metabolic analysis, availability of these key intermediates for amino acid biosynthesis was restricted in reddish cells since they were preferentially funnelled into fatty acid and astaxanthin

biosynthetic pathways.

Histidine was the only amino acid that was at an apparent higher level in reddish than in green cells. Under the conditions used for quantification, the retention time for histidine was coincident with that for γ-aminobutyric acid (GABA), a compound that has been described to accumulate in *Haematococcus* under N limitation (Recht et al., 2014). This prevented to discern whether the observed increase was due to a boost in histidine, GABA, or the sum of both.

In reddish *Haematococcus* cells amino acids could be used as precursors for TCA cycle intermediates or pyruvate, through transamination reactions. Our transcriptomic analysis showed that alanine aminotransferase (ALT) gene was slightly activated in reddish cells, allowing a preferential conversion of alanine into pyruvate, as suggested the lower alanine content (52% less than green cells). The gene coding for aspartate aminotransferase (AAT) was 4-fold up-regulated in reddish cells, which could account for a 3-fold lower aspartate content probably associated to enhanced provision of OAA for TCA cycle.

The higher transcription level of the genes that codify for nitrate/nitrite transporter (NRT) as well as for nitrate reductase (NR), Table 3, indicates that reddish cells are adapted to handle low nitrate level both outside and inside the cell. Regarding incorporation of the ammonia resulting from the reduction of nitrate into carbon skeletons, via GS/GOGAT, the transcription level of the gene codifying for glutamine synthetase (GS) was higher in reddish than in green cells, whereas that for glutamate synthase (GOGAT) was virtually the same in both cell types, Table 3. Glutamate and glutamine content were 34% and 44% lower than in green cells, respectively.

3.7. TCA cycle flux in Haematococcus is enhanced during astaxanthin accumulation

The transcription of genes that codify several enzymes of the TCA cycle, such as citrate synthase (CS), aconitase (ACO), isocitrate dehydrogenase (IDH), 2-oxoglutarate dehydrogenase (OGDH) and succinilCoA synthetase (SCS) were higher in reddish cells when compared to green cells, Fig. 4. Likewise, levels of TCA cycle intermediates (OAA, 2-oxoglutarate, succinate, fumarate and malate) were lower in reddish, highlighting a 2.5-fold drop in 2-oxoglutarate, likely due to enhanced conversion into glutamate by the activated GS, Table 3. This behaviour has also been reported for *C. reinhardtii* under N starvation conditions (Bölling and Fiehn, 2005).

Our integrative analysis indicate that the flux of TCA cycle in *Haematococcus* can be enhanced during astaxanthin accumulation, in line with the proposal of Recht et al. (2014). Regarding the content in TCA intermediates, only that of citrate was higher in reddish that in green cells, Table 3. Excess citrate has been described for *C. reinhardtii* subjected to N starvation, and correlated with the increase in lipid storage (Wase et al., 2014)

Expression of the gene codifying for phosphoenolpyruvate carboxylase (PEPC), that catalyses the conversion of pyruvate to OAA, was higher in reddish cells, suggesting again activation of the TCA cycle.

4. Conclusions

The suitability of vegetative reddish palmelloid cells as a model system to clarify the regulation of astaxanthin synthesis and accumulation in *Haematococcus* has been verified. Data from both metabolomic and transcriptomic analyses have been integrated and compared to those for green cells. A massive metabolic reprogramming was unveiled for the reddish cells, involving differential expression of hundreds of genes and affecting key pathways converging into astaxanthin biosynthesis and storage. Besides, a major advance has been made in discerning the underlying control mechanisms, having identified the bHLH transcription factor family and specific promoter sequences as putative regulators of astaxanthin biosynthesis.

5. Data and code availability

The RNA-seq datasets generated in this study have been deposited in the Gene Expression Omnibus (GEO) under accession GSE161337. Several custom R scripts and packages that were used to analyse the data generated in this study were deposited in the GitHub repository https://github.com/ABRomeroLosada/tartessos_RNAseq

6. Formatting of funding sources

This work was supported by Intramural Action of the Spanish National Research Council (201420E035) and the research project MINOTAUR (BIO2017-84066-R) from Spanish Ministry of Science and Innovation.

CRediT authorship contribution statement

Cristina Hoys: Investigation, Methodology. **Ana B. Romero-Losada:** Investigation, Methodology, Data curation, Software. **Esperanza del Río:** Conceptualization, Supervision, Writing - review & editing. **Miguel G. Guerrero:** Conceptualization, Supervision, Writing - review & editing. **Francisco J. Romero-Campero:** Data curation, Formal analysis, Software, Writing - original draft, Writing - review & editing. **Mercedes García-González:** Conceptualization, Project administration, Resources, Writing - original draft, Writing - review & editing.

Declaration of Competing Interest

The authors declare that they have no known competing financial interests or personal relationships that could influence the work reported in this paper. Miguel G. Guerrero declares that he is a shareholder and board member of AlgaEnergy, S.A.

Appendix A. Supplementary data

Supplementary data to this article can be found online at https://doi.org/10.1016/j.biortech.2021.125150.

References

Bailey, T.L., Boden, M., Buske, F.A., Frith, M., Grant, C.E., Clementi, L., Ren, J., Li, W.W., Noble, W.S., 2009. MEME SUITE: tools for motif discovery and searching. Nucleic Acids Res. 37, W202–W208. https://doi.org/10.1093/nar/gkp335.

Bölling, C., Fiehn, O., 2005. Metabolite profiling of Chlamydomonas reinhardtii under nutrient deprivation. Plant Physiol. 139, 1995–2005. https://doi.org/10.1104/pp.105.071589.

Chen, G., Wang, B., Han, D., Sommerfeld, M., Lu, Y., Chen, F., Hu, Q., 2015. Molecular mechanisms of the coordination between astaxanthin and fatty acid biosynthesis in Haematococcus pluvialis (Chlorophyceae). Plant J. 81, 95–107. https://doi.org/10.1111/tpj.12713.

Del Campo, J.A., Rodríguez, H., Moreno, J., Vargas, M.Á., Rivas, J., Guerrero, M.G., 2004. Accumulation of astaxanthin and lutein in Chlorella zofingiensis (Chlorophyta). Appl. Microbiol. Biotechnol. 64, 848–854. https://doi.org/10.1007/s00253-003-1510-5.

Del Río, E., Acién, F.G., García-Malea, M.C., Rivas, J., Molina-Grima, E., Guerrero, M.G., 2005. Efficient one-step production of astaxanthin by the microalga Haematococcus pluvialis in continuous culture. Biotechnol. Bioeng. 91, 808–815. https://doi.org/10.1002/bit.20547.

Del Río, E., Acién, F.G., Guerrero, M.G., 2010. Photoautotrophic production of astaxanthin by the microalga Haematococcus pluvialis. In: Sustainable Biotechnology. Springer, Netherlands, Dordrecht, pp. 247–258. https://doi.org/10.1007/978-90-481-3295-9_13.

Del Río, E., Armendáriz, A., García-Gómez, E., García-González, M., Guerrero, M.G., 2015. Continuous culture methodology for the screening of microalgae for oil. J. Biotechnol. 195, 103–107. https://doi.org/10.1016/j.jbiotec.2014.12.024.

Fábregas, J., Otero, A., Maseda, A., Domínguez, A., 2001. Two-stage cultures for the production of Astaxanthin from Haematococcus pluvialis. J. Biotechnol. 89, 65–71. https://doi.org/10.1016/S0168-1656(01)00289-9.

Fang, L., Zhang, J., Fei, Z., Wan, M., 2020. Astaxanthin accumulation difference between non-motile cells and akinetes of Haematococcus pluvialis was affected by pyruvate metabolism. Bioresour. Bioprocess. 7, 5. https://doi.org/10.1186/s40643-019-0293-1.

Franco-Zorrilla, J.M., López-Vidriero, I., Carrasco, J.L., Godoy, M., Vera, P., Solano, R., 2014. DNA-binding specificities of plant transcription factors and their potential to

define target genes. Proc. Natl. Acad. Sci. 111, 2367–2372. https://doi.org/10.1073/pnas.1316278111.
Frazee, A.C., Pertea, G., Jaffe, A.E., Langmead, B., Salzberg, S.L., Leek, J.T., 2015. Ballgown bridges the gap between transcriptome assembly and expression analysis. Nat. Biotechnol. 33, 243–246. https://doi.org/10.1038/nbt.3172.
Gao, Z., Li, Y., Wu, G., Li, G., Sun, H., Deng, S., Shen, Y., Chen, G., Zhang, R., Meng, C., Zhang, X., 2015. Transcriptome analysis in haematococcus pluvialis: astaxanthin induction by salicylic acid (SA) and Jasmonic Acid (JA). PLoS One 10, e0140609. https://doi.org/10.1371/journal.pone.0140609.
Gao, Z., Meng, C., Gao, H., Zhang, X., Xu, D., Su, Y., Wang, Y., Zhao, Y., Ye, N., 2013. Analysis of mRNA expression profiles of carotenogenesis and astaxanthin production of Haematococcus pluvialis under exogenous 2, 4-epibrassinolide (EBR). Biol. Res. 46, 201–206. https://doi.org/10.4067/S0716-97602013000200012.
García-Cubero, R., Moreno-Fernández, J., Acién-Fernández, F.G., García-González, M., 2018. How to combine CO2 abatement and starch production in Chlorella vulgaris. Algal Res. 32, 270–279. https://doi.org/10.1016/J.ALGAL.2018.04.006.
García-Malea, M.C., Gabriel Acién, F., Río, E.D., Fernández, J.M., Cerón, M.C., Guerrero, M.G., Molina-Grima, E., 2009. Production of astaxanthin by haematococcus Pluvialis: taking the one-step system outdoors. Biotechnol. Bioeng. 102, 651–657. https://doi.org/10.1002/bit.22076.
Grünewald, K., Hirschberg, J., Hagen, C., 2001. Ketocarotenoid biosynthesis outside of plastids in the unicellular green alga Haematococcus pluvialis. J. Biol. Chem. 276, 6023–6029. https://doi.org/10.1074/jbc.M006400200.
Guerin, M., Huntley, M.E., Olaizola, M., 2003. Haematococcus astaxanthin: applications for human health and nutrition. Trends Biotechnol. 21, 210–216. https://doi.org/10.1016/S0167-7799(03)00078-7.
Gwak, Y., Hwang, Y., Wang, B., Kim, M., Jeong, J., Lee, C.-G., Hu, Q., Han, D., Jin, E., 2014. Comparative analyses of lipidomes and transcriptomes reveal a concerted action of multiple defensive systems against photooxidative stress in Haematococcus pluvialis. J. Exp. Bot. 65, 4317–4334. https://doi.org/10.1093/jxb/eru206.
Haas, B.J., Papanicolaou, A., Yassour, M., Grabherr, M., Blood, P.D., Bowden, J., Couger, M.B., Eccles, D., Li, B., Lieber, M., MacManes, M.D., Ott, M., Orvis, J., Pochet, N., Strozzi, F., Weeks, N., Westerman, R., William, T., Dewey, C.N., Henschel, R., LeDuc, R.D., Friedman, N., Regev, A., 2013. De novo transcript sequence reconstruction from RNA-seq using the Trinity platform for reference generation and analysis. Nat. Protoc. 8, 1494–1512. https://doi.org/10.1038/nprot.2013.084.
He, B., Hou, L., Dong, M., Shi, J., Huang, X., Ding, Y., Cong, X., Zhang, F., Zhang, X., Zang, X., 2018. Transcriptome analysis in Haematococcus pluvialis: Astaxanthin induction by high light with acetate and Fe2+. Int. J. Mol. Sci. 10.3390/ijms19010175.
Heinrikson, R.L., Meredith, S.C., 1984. Amino acid analysis by reverse-phase high-performance liquid chromatography: Precolumn derivatization with phenylisothiocyanate. Anal. Biochem. 136, 65–74. https://doi.org/10.1016/0003-2697(84)90307-5.
Hoskisson, P.A., Hobbs, G., 2005. Continuous culture – making a comeback? Microbiology 151, 3153–3159. https://doi.org/10.1099/mic.0.27924-0.
Hu, C., Cui, D., Sun, X., Shi, J., Xu, N., 2020. Primary metabolism is associated with the astaxanthin biosynthesis in the green algae Haematococcus pluvialis under light stress. Algal Res. 46, 101768 https://doi.org/10.1016/j.algal.2019.101768.
Huerlimann, R., Heimann, K., 2013. Comprehensive guide to acetyl-carboxylases in algae. Crit. Rev. Biotechnol. 33, 49–65. https://doi.org/10.3109/07388551.2012.668671.
Jin, J., Tian, F., Yang, D.C., Meng, Y.Q., Kong, L., Luo, J., Gao, G., 2017. PlantTFDB 4.0: Toward a central hub for transcription factors and regulatory interactions in plants. Nucleic Acids Res. 10.1093/nar/gkw982.
Kim, D., Paggi, J.M., Park, C., Bennett, C., Salzberg, S.L., 2019. Graph-based genome alignment and genotyping with HISAT2 and HISAT-genotype. Nat. Biotechnol. 37, 907–915. https://doi.org/10.1038/s41587-019-0201-4.
Kovaka, S., Zimin, A.V., Pertea, G.M., Razaghi, R., Salzberg, S.L., Pertea, M., 2019. Transcriptome assembly from long-read RNA-seq alignments with StringTie2. Genome Biol. 20, 278. https://doi.org/10.1186/s13059-019-1910-1.
Lee, C., Choi, Y.-E., Yun, Y.-S., 2016. A strategy for promoting astaxanthin accumulation in Haematococcus pluvialis by 1-aminocyclopropane-1-carboxylic acid application. J. Biotechnol. 236, 120–127. https://doi.org/10.1016/j.jbiotec.2016.08.012.
Lu, Z., Dai, J., Zheng, L., Teng, Z., Zhang, Q., Qiu, D., Song, L., 2020. Disodium 2-oxo-glutarate promotes carbon flux into astaxanthin and fatty acid biosynthesis pathways in Haematococcus. Bioresour. Technol. 299, 122612 https://doi.org/10.1016/j.biortech.2019.122612.
Lv, H., Xia, F., Liu, M., Cui, X., Wahid, F., Jia, S., 2016. Metabolomic profiling of the astaxanthin accumulation process induced by high light in Haematococcus pluvialis. Algal Res. 20, 35–43. https://doi.org/10.1016/j.algal.2016.09.019.
Malinova, I., Alseekh, S., Feil, R., Fernie, A.R., Baumann, O., Schöttler, M.A., Lunn, J.E., Fettke, J., 2017. Starch synthase 4 and plastidal phosphorylase differentially affect starch granule number and morphology. Plant Physiol. 174, 73–85. https://doi.org/10.1104/pp.16.01859.
Mistry, J., Finn, R.D., Eddy, S.R., Bateman, A., Punta, M., 2013. Challenges in homology search: HMMER3 and convergent evolution of coiled-coil regions. Nucleic Acids Res. https://doi.org/10.1093/nar/gkt263.
Morimoto, D., Yoshida, T., Sawayama, S., 2020. Draft genome sequence of the astaxanthin-producing microalga Haematococcus lacustris strain NIES-144. Microbiol. Resour. Announc. 9 https://doi.org/10.1128/MRA.00128-20.
Moriya, Y., Itoh, M., Okuda, S., Yoshizawa, A.C., Kanehisa, M., 2007. KAAS: an automatic genome annotation and pathway reconstruction server. Nucleic Acids Res. https://doi.org/10.1093/nar/gkm321.
O'Malley, R.C., Huang, S.C., Song, L., Lewsey, M.G., Bartlett, A., Nery, J.R., Galli, M., Gallavotti, A., Ecker, J.R., 2016. Cistrome and epicistrome features shape the regulatory DNA landscape. Cell 166, 1598. https://doi.org/10.1016/j.cell.2016.08.063.
Recht, L., Töpfer, N., Batushansky, A., Sikron, N., Gibon, Y., Fait, A., Nikoloski, Z., Boussiba, S., Zarka, A., 2014. Metabolite profiling and integrative modeling reveal metabolic constraints for carbon partitioning under nitrogen starvation in the green algae Haematococcus pluvialis. J. Biol. Chem. 289, 30387–30403. https://doi.org/10.1074/jbc.M114.555144.
Recht, L., Zarka, A., Boussiba, S., 2012. Patterns of carbohydrate and fatty acid changes under nitrogen starvation in the microalgae Haematococcus pluvialis and Nannochloropsis sp. Appl. Microbiol. Biotechnol. 94, 1495–1503. https://doi.org/10.1007/s00253-012-3940-4.
Ritchie, M.E., Phipson, B., Wu, D., Hu, Y., Law, C.W., Shi, W., Smyth, G.K., 2015. Limma powers differential expression analyses for RNA-sequencing and microarray studies. Nucleic Acids Res. https://doi.org/10.1093/nar/gkv007.
Rodrigues-Pousada, C.A., Nevitt, T., Menezes, R., Azevedo, D., Pereira, J., Amaral, C., 2004. Yeast activator proteins and stress response: an overview. FEBS Lett. 567, 80–85. https://doi.org/10.1016/j.febslet.2004.03.119.
Roessner, U., Luedemann, A., Brust, D., Fiehn, O., Linke, T., Willmitzer, L., Fernie, A.R., 2001. Metabolic profiling allows comprehensive phenotyping of genetically or environmentally modified plant systems. Plant Cell 13, 11–29. https://doi.org/10.1105/tpc.13.1.11.
Römer, S., Fraser, P.D., 2005. Recent advances in carotenoid biosynthesis, regulation and manipulation. Planta 221, 305–308. https://doi.org/10.1007/s00425-005-1533-5.
Shah, M.M.R., Liang, Y., Cheng, J.J., Daroch, M., 2016. Astaxanthin-producing green microalga Haematococcus pluvialis: from single cell to high value commercial products. Front. Plant Sci. 7, 531. https://doi.org/10.3389/fpls.2016.00531.
Solovchenko, A.E., 2015. Recent breakthroughs in the biology of astaxanthin accumulation by microalgal cell. Photosynth. Res. 125, 437–449. https://doi.org/10.1007/s11120-015-0156-3.
Toledo-Ortiz, G., Johansson, H., Lee, K.P., Bou-Torrent, J., Stewart, K., Steel, G., Rodríguez-Concepción, M., Halliday, K.J., 2014. The HY5-PIF regulatory module coordinates light and temperature control of photosynthetic gene transcription. PLoS Genet. 10, e1004416 https://doi.org/10.1371/journal.pgen.1004416.
Veyel, D., Erban, A., Fehrle, I., Kopka, J., Schroda, M., 2014. Rationales and approaches for studying metabolism in eukaryotic microalgae. Metabolites. https://doi.org/10.3390/metabo4020184.
Vidhyavathi, R., Venkatachalam, L., Sarada, R., Ravishankar, G.A., 2008. Regulation of carotenoid biosynthetic genes expression and carotenoid accumulation in the green alga Haematococcus pluvialis under nutrient stress conditions. J. Exp. Bot. 59, 1409–1418. https://doi.org/10.1093/jxb/ern048.
Wase, N., Black, P.N., Stanley, B.A., Dirusso, C.C., 2014. Integrated quantitative analysis of nitrogen stress response in Chlamydomonas reinhardtii using metabolite and protein profiling. J. Proteome Res. 13, 1373–1396. https://doi.org/10.1021/pr400952z.
Wen, Z., Liu, Z., Hou, Y., Liu, C., Gao, F., Zheng, Y., Chen, F., 2015. Ethanol induced astaxanthin accumulation and transcriptional expression of carotenogenic genes in Haematococcus pluvialis. Enzyme Microb. Technol. 10.1016/j.enzmictec.2015.06.010.
Yu, G., Wang, L.-G., Han, Y., He, Q.-Y., 2012. clusterProfiler: an R package for comparing biological themes among gene clusters. Omi. A J. Integr. Biol. 16, 284–287. https://doi.org/10.1089/omi.2011.0118.